Role of the stratosphere in Northern winter climate change as simulated by the CMIP5 models

Elisa Manzini[(1)], Alexey Yu. Karpechko[(2)], James Anstey[(3)], Mark P. Baldwin[(4)], Thomas Birner[(5)], Robert X. Black[(6)], Chiara Cagnazzo[(7,8)], Natalia Calvo[(9,10)], Andrew Charlton-Perez[(11)], Bo Christiansen[(12)], Paolo Davini[(13,8)], Ed Gerber[(14)], Marco Giorgetta[(1)], Lesley Gray[(3)], Steven Hardiman[(15)], Yun-Young Lee[(6)], Dan Marsh[(10)], Brent A McDaniel[(16)], Lorenzo Polvani[(17)], Ariaan Purich[(18)], Adam A. Scaife[(15)], Drew Shindell[(19)], Seok-Woo Son[(18)], Evgeny Volodin[(20)], Shingo Watanabe[(21)], John Wilson[(22)], Seiji Yukimoto[(23)], Giuseppe Zappa[(11)]

Corresponding author: Elisa Manzini (elisa.manzini@zmaw.de)

2012/07

[(1)] Max Planck Institute for Meteorology, Hamburg, Germany

[(2)] Finnish Meteorological Institute, Helsinki, Finland

[(3)] University of Oxford, Oxford, UK

[(4)] University of Exeter, Exeter, UK

[(5)] Colorado State University, Fort Collins, CO, USA

[(6)] Georgia Institute of Technology, Atlanta, GA, USA

[(7)] Istituto di Scienze dell'Atmosfera e del Clima, Consiglio Nazionale delle Ricerche, Roma, Italy

[(8)] Centro Euro-Mediterraneo per i Cambiamenti Climatici, Bologna, Italy

[(9)] Universidad Complutense de Madrid, Madrid, Spain

[(10)] National Center for Atmospheric Research, Boulder, CO, USA

[11] University of Reading, Reading, UK

[12] Danish Meteorological Institute, Copenhagen, Denmark

[13] Università Ca' Foscari, Venezia, Italia

[14] New York University, New York, USA

[15] Met Office Hadley Center, Exeter, UK

[16] Kennesaw State University

[17] Columbia University, New York, USA

[18] McGill University, Montreal, Quebec, Canada

[19] Goddard Institute for Space Studies, NASA, New York, USA

[20] Institute of Numerical Mathematics, Moscow, Russia

[21] Japan Agency for Marine-Earth Science and Technology, Yokohama, Japan

[22] Geophysical Fluid Dynamics Laboratory, Princeton, NJ, USA

[23] Meteorological Research Institute, Tsukuba, Japan

Abstract

Stratospheric climate change and its potential for surface climate change as simulated by the Coupled Model Intercomparison Project – phase 5 (CMIP5) model ensemble are assessed. We focus on Northern winter climate projections for the period 1961 to 2100. The results confirm previous projections that winds in the polar lower stratosphere will weaken at high latitudes and strengthen at low latitudes by the end of the century. To categorize the models as high- or low-top based on the location of the model lid does not reveal significant differences in polar winter stratospheric change. While the majority of high-top models exhibit a significantly larger tropical tropospheric warming than low-top models, this result does not appear to be related to differences in stratospheric processes and vertical resolution. We find that the CMIP5 models are more usefully subdivided depending upon the projected winter polar stratospheric change. Sea level pressure changes that are consistent with a weakening of the high latitude stratospheric winds and an increased Brewer-Dobson circulation are in this way revealed. Corresponding changes are also evident in tropospheric intra-seasonal phenomena. We conclude that the change in the strength of the winter stratospheric polar vortex can be an important factor for the projection of the surface changes. Nevertheless, the spread of the modeled stratospheric polar changes within the CMIP5 models calls for a better understanding of the relative role and interdependence of stratospheric dynamical processes and other factors in leading to the reported mean changes.

1. Introduction

There is evidence that future changes to the stratosphere could have an important impact on tropospheric climate change in the Northern Hemisphere (NH), from the early modeling work by *Shindell et al.* [1999] to more recent analyses including high/low top models in combination with multi-model ensembles [*Scaife et al.,* 2012], boundary-controlled experiments with a single pair of high/low top models [*Karpechko and Manzini,* 2012], and experiments aimed at testing the sensitivity to the basic state [*Sigmond and Scinocca,* 2010]. These and other related studies aim to answer two important questions:

- What is the connection, on climate time scales, between changes in the stratospheric polar vortex and the NH tropospheric circulation?
- What are the processes responsible for this connection?

With increasing greenhouse gases, the winter stratospheric polar vortex is expected to respond to local changes in radiative forcing (stratospheric cooling) as well as to remote tropospheric changes in wave forcing and/or changes in wave propagation between the troposphere and the stratosphere [*Sigmond et al*., 2004; *McLandress and Shepherd,* 2009; *Bell et al.,* 2010; among others]. Although future projections of the NH winter lower stratosphere differ in many aspects, the consistent response that appears to emerge is that the zonal winds will weaken at high latitudes and strengthen at low latitudes, a change that can be interpreted as an expansion of the stratospheric vortex. The polar weakening of the stratospheric winds is consistent with the strengthened Brewer-Dobson (BD) circulation in response to climate change widely reported to occur in models in response to increased greenhouse gas concentrations [*Butchart and Scaife,* 2001; *Butchart et al.,* 2006; 2010, *Shepherd and McLandress*, 2011; *Garcia and Randel*, 2008; *Calvo and Garcia,* 2009]. A combination of weakened polar stratospheric zonal winds and strengthened BD imply that dynamical processes (wave drag/forcing, e.g. *Andrews et al.* [1987]) are implicated in the stratospheric response to climate change.

The works by *Sigmond et al*. [2004] and *Bell* [2009] have demonstrated the possibility that the stratospheric polar vortex can respond remotely to changes in tropospheric dynamics as a result of greenhouse gas forcing. The weakening of the stratospheric polar winds under increased CO_2 has been found in controlled experiments, which excluded local radiative forcing in the stratosphere [*Sigmond et al.,* 2004; *Bell,* 2009]. *Sigmond et al.* [2004] carried out numerical experiments with a middle atmosphere model, where the CO_2 was doubled only in the troposphere, and obtained a dipole zonal wind response, with negative change at the high latitudes, largest in the upper stratosphere. The dipole wind response did not occur in a complementary experiment where the CO_2 was doubled only in the stratosphere and mesosphere. *Bell* [2009] found a similar dipole pattern in stratospheric zonal wind response (with the same polarity) in sensitivity experiments to a sea surface temperature representative of CO_2 quadrupling.

Concerning the surface impact of the changes in the stratospheric polar vortex, both the works by *Scaife et al.* [2012] and *Karpechko and Manzini* [2012] report that using models with tops above the stratopause in climate change experiments has the effect of reducing the projected changes in sea level pressure both in the Arctic and at mid-latitudes that are found in standard (lower top) climate models. These effects are consistent with a stronger Equator-to-pole BD circulation and the downward influence of intra-seasonal stratospheric anomalies seen in observations [*Baldwin and Dunkerton,* 2001]. The results of the high top versus low top comparisons by *Scaife et al*. [2012] and *Karpechko and Manzini* [2012] therefore support the notion that stratospheric changes can be different in high top models, because stratospheric dynamical processes are better represented in the high top models.

The purpose of this paper is to assess the stratospheric changes and their associated surface signatures in the Coupled Model Intercomparison Project – phase 5 (CMIP5) ensembles of models, for the period 1960 to 2100. We focus on changes to the NH stratospheric polar vortex and the potential impact of the stratospheric changes at the surface. The multi-model approach is used here to identify robust responses between the models. The specific questions addressed are:

- Are the projected changes in the NH stratospheric polar vortex consistent among the CMIP5 models?
- What are the consequences of the stratospheric changes for Northern hemisphere surface climate change?

The CMIP5 dataset provides us, for the first time, with the possibility to assess climate change in the stratosphere from a multi-model ensemble of coupled atmosphere-ocean-sea ice models. This is because in the design of the CMIP5 experiments attention has been paid to the specification of forcings of stratospheric change (such as ozone trends) and also because of genuine improvements in the representation of stratospheric processes with respect to previous CMIP model ensembles.

An assessment of the representation of stratospheric processes in the CMIP5 ensemble of models has been reported by *Charlton-Perez et al.* [2012]. By sub-setting CMIP5 models with respect to the location of their atmospheric model top, *Charlton-Perez et al*. [2012] found that:

- Stratospheric variability at all time scales is better simulated in the CMIP5 models with tops above the stratopause.
- The mean climate and historical trends among the CMIP5 models are not distinguishable simply on the basis of a model top characterization above /below the stratopause.

The *Charlton-Perez et al.* [2012] assessment also shows an improvement in the representation of the stratospheric mean flow in CMIP5 models as compared to the CMIP3 (Coupled Model Intercomparison Project – phase 3) models.

The organization of the paper is as follows. In section 2 the methodology is described. Section 3 compares the response to increased CO_2 concentrations in both the CMIP3 and CMIP5 sets of available models, without distinction of the model top location. This links to previous literature and documents the overall differences emerging from the two datasets, with a focus on the stratosphere. Experiments with 1 percent per year increase in CO_2 are used to compare the two generations of model sets, since this was common to both CMIP3 and CMIP5, and provides the response to identical radiative forcing without the complications of additional forcing, such as aerosols, land-use and ozone forcing.

In sections 4 and 5 results from the CMIP5 historical and RCP8.5 scenarios (see section 2) are used to characterize the stratosphere and its potential role in climate projections. The analysis focuses on the winter season, the time of the year when stratospheric – tropospheric dynamical coupling is known to be active [*Baldwin and Dunkerton,* 2001] and examines changes in the mean state (section 4) and intra-seasonal variations (section 5).

2. Methodology

CMIP3 / CMIP5 multi-model inter-comparisons are carried out (section 3) employing simulations in which the CO2 concentrations are increased by 1% per year (hereafter denoted 1pctCO2). The experiments are initialized from pre-industrial control runs and are continued for 140 years, reaching 4xCO2 levels by the end of the simulations. The purpose of examining these simulations is the analysis of transient climate sensitivity, evaluation of model responses for one idealized forcing, and comparison with previous CMIPs. Because of the idealized nature of these runs, differences between the average of years 101-140 and years 1-40 are analysed. The average difference in CO2 forcing between these two 40-year means is about 3xCO2. To interpret the results of the 1pctCO2 runs, one also must keep in mind that this is a transient run with a very rapid increase in CO_2, which means that the ocean state is y far from being in equilibrium with the radiative forcing from the CO_2 increase. The stratospheric response can be affected by the different sea surface temperature forcing than is the case for a more equilibrated simulation. For this analysis, outputs for 12 CMIP3 models and 11 CMIP5 models were available (Table 1).

To characterize the CMIP5 simulations stratosphere and its potential role in climate projections (sections 4, 5), the historical simulations from 1961 are employed together with the Representative Concentration Pathways 8.5 scenario (RCP8.5), in which year-2100 has a nominal radiative forcing of 8.5 Wm^{-2} [*Van Vuuren et al.,* 2011]. Differences between averages of the RCP8.5 period 2061-2100 minus the historical period 1961-2000 are examined. The model output used are reported in Table 2, classified by high and low top as in *Charlton-Perez et al.* [2012]: Models with tops below/above the stratopause (nominally located at 1 hPa) are classified low/high top, respectively. The separation is motivated by the assumption that the high-top models more realistically include stratospheric processes, for instance planetary wave dissipation whose breaking level is typically located close to the stratopause. If there were no other differences between the two ensembles, the difference in climate simulations between the ensembles could be attributed to the stratospheric processes. The CanESM2 model, with top at 1 hPa, is excluded in the difference plots between high and low top models. Table 3 provides a summary of the CMIP5 models by diagnostic, and shows how many realizations per model and diagnostic are used. When more than one realization from a given model is used, it is first averaged across all realizations of a given model before calculating the multi-model mean.

2.1 Inter-model consistency and statistical significance

In reporting results from projections of future changes from a multi-model ensemble it is important to have information on the level of inter-model agreement in the future changes. To address this question, attention is paid to the consistency in the sign of the projected change as been done previously, for example in comparisons of precipitation projections [*Solomon et al.,* 2007]. When differences in the projected changes between two multi-model averages are shown, then 2-tailed t-test statistical significance is reported. This latter addresses the question of whether there is enough evidence to reject the null-hypothesis that the projections of the two multi-model ensemble averages are the same.

3. Inter-comparison of CMIP3 and CMIP5 simulations

In this section we carry out a comparison of the CMIP3 and CMIP5 1%/yr increase in CO2 concentration experiments. Figure 1a-c shows the projected change in zonal mean zonal winds due to the approximately x3 increase in CO2 concentrations (see methods section). As seen in previous studies (e.g. *Scaife et al.* [2012] and references therein) both CMIP3 and CMIP5 models show a dipole structure with weakening at high latitudes and strengthening at low latitudes in the troposphere. However, in the lower stratosphere (200-10 hPa, poleward of 50^{o}N) the wind changes are qualitatively and quantitatively different. In CMIP3 the strengthening of the zonal winds extends to the North Pole but in CMIP5 it is abruptly halted between 60^{o}-70^{o}N and there is an easterly change (weakening) at high latitudes, so that the polar weakening extends throughout the depth of the troposphere and stratosphere in the CMIP5 runs, in contrast to the CMIP3 runs. The tropospheric signal is also strengthened in the CMIP5 runs. The inter-model consistency in the sign of the response in given by the shading:

for at least 66% of the models the zonal wind response is negative poleward of 70^{o}N in CMIP5, while it is positive for the same fraction of models in CMIP3. The CMIP5-CMIP3 difference (Figure 1c) is therefore also characterized by a dipole in the stratosphere, with positive/negative difference equatorward / poleward of 50^{o}N. For the models considered, the CMIP5-CMIP3 difference poleward of 60^{o}N is significant in the lower stratosphere (200-50 hPa). At 80^{o}N, 10 hPa, the CMIP5-CMIP3 difference is of the same size as the CMIP3 response.

The change in the atmospheric temperature in both the CMIP5 and CMIP3 sets is characterized by the typical warming in the troposphere and cooling in the stratosphere [*IPCC* 2007]. In Figure 1d the CMIP5 minus CMIP3 difference in the NH zonal mean temperature change is shown. The dipole stratospheric (100-10 hPa) temperature difference in the change is consistent with the zonal wind difference. Cooling in the tropics and warming in the polar region in CMIP5 with respect to CMIP3, imply a stronger Equator-to-pole BD circulation response in CMIP5. Stratospheric dynamical processes (i.e., variability of the stratospheric vortex) appear therefore to be implicated in the CMIP5-CMIP3 differences. In the tropical troposphere, the CMIP5-CMIP3 temperature difference is less than 0.5 K, and indicates that the average difference in climate sensitivity between the two sets of models is not significant. At the surface, the polar warming (60-80N) is quite possibly due to advances in the representation of seaice processes in CMIP5 with respect to CMIP3, although improved vertical interaction between the stratospheric and sea-ice processes cannot be ruled out [*Hardiman et al.* 2012].

Figures 1e and f show respectively the SLP change in CMIP5 and the CMIP5-CMIP3 difference in the change. The CMIP5 ensemble SLP change is characterized by the well know pattern of negative changes over the pole and positive changes at mid-latitude [*IPCC* 2007]. The pattern of the CMIP5-CMIP3 difference in SLP change, positive over the Arctic and negative around it, is consistent with the changes in CMIP5-CMIP3 zonal winds in the stratosphere and the signal of polar stratospheric change shown by *Scaife et al.* [2012] and *Karpechko and Manzini* [2012], although it is not statistically significant at $p<0.1$. In JFM (not shown) the CMIP5-CMIP3 difference over the Arctic is broader and significant (2-tailed t-test, $p<0.1$), consistent with the results by *Karpechko and Manzini* [2012] who found that the stratospheric influence maximizes in late winter-early spring. Compared with the previously reported analysis, the positive polar SLP difference shown in Figure 1f is however limited to higher latitudes. Different from previous studies, the stratospheric impact shown in Figure 1 is estimated by means of a multi-model mean. It is therefore likely that the inter-model spread related to the representation of all climate processes (e.g., within the troposphere, ocean, sea-ice, not only stratosphere) is responsible for the high latitude confinement of the positive polar SLP CMIP5-CMIP3 difference.

4. CMIP5 projections: Mean Changes

In this section, future climate change is diagnosed from the historical and RCP8.5 scenarios of the CMIP5 simulations which include all known natural and anthropogenic forcings, in contrast to the 1%/yr CO_2 increase experiments discussed in the previous section. The future projection of zonally-averaged stratospheric zonal winds (Figure 2a) shows a dipole pattern similar to that in Figure 1a. At low latitudes the winds strengthen around the tropopause, consistently with the well known upward (and poleward) shift and the strengthening of the subtropical tropospheric jet [*IPCC* 2007]. At high latitudes the zonal wind change is negative from the surface to the middle stratosphere (10 hPa). The inter-model consistency in the sign of the response in given by the shading. The negative change poleward of 60^{o}N occurs for at least 66% of the models in the middle stratosphere 10-50 hPa and for more that 90% of the models in the lower stratosphere and the troposphere (below 100hPa). Both the low latitude positive changes and high latitude negative changes are larger in magnitude in the CMIP5 high top models (Figure 2b). However, significant changes are found primarily only at low latitudes. In addition, Figure 2b shows hints of significant dipole-like difference in the tropospheric wind strength.

Figures 2c and 2d show corresponding diagnoses for zonally-averaged temperatures. The change in zonal mean temperature in the CMIP5 multi-model ensemble mean is characterized by the typical warming in the troposphere and cooling in the stratosphere [*IPCC* 2007]. The difference between high and low top models (Figure 2d) reveals significant changes in the tropical troposphere, indicating larger tropospheric warming. This result is consistent with the low latitude positive changes in zonal mean zonal wind (Figure 2b) and is discussed further below. At high latitudes, the CMIP5 high-top minus low-top difference in the stratospheric change shows greater cooling/warming below/above ~70hPa, but the signals have low statistical significance.

At the surface (Figure 2e), the CMIP5 multi model mean change in SLP reproduces the well-known pattern of decreased SLP over the pole and increases at mid-latitudes.

The SLP difference CMIP5 high-top minus CMIP5 low-top models (Figure 2f) is however not consistent with the high latitude stratospheric changes in zonal mean zonal wind (Figure 2b), because it shows a significant decrease of the polar SLP, surrounded by higher pressure at mid-latitudes. In addition, as noted previously, the high-top minus low-top comparison reveals stronger subtropical zonal mean zonal winds (Figure 2b) and higher tropospheric zonal mean temperatures in the high-top models (Figure 2d). These results are absent in Figures 1c and 1d, and cast doubts that the SLP difference between the two ensembles are attributable to stratospheric changes.

Figure 3 explores in more detail the fact shown in Figure 2b and 2d that the CMIP5 high top models appear to have a larger tropospheric warming in response to climate change and its consequences on SLP surface change. Figure 3a shows a scatter plot of the projected temperature change in the tropics at 300 hPa compared with that at 850 hPa. It shows that the models with a large warming in the upper tropical troposphere (300 hPa) also have a large warming in the lowermost troposphere (850 hPa). This is consistent with the expectation of how the tropical troposphere responds to the greenhouse gases increase, and has been shown previously [*Gettelman and Fu,* 2008]. Clearly, Figure 3a shows that the majority of the high-top models are warming at a faster rate than the majority of the low-top models also in the lower troposphere, suggesting that the high-top models have, on average, larger climate sensitivity than the low-top models. It is not clear at this point, what might be the origin of these different responses in tropical (and global, not shown) tropospheric warming between the high and low top models. However, Figure 3a also shows that although as a group the high and low top models shows a distinct difference in their tropospheric warming, the 3 pairs of high and low-top models that share the same tropospheric component (shown by filled squares, from top to bottom: EC-EARTH, CMCC-CESM and HadGEM2-CC/ES) have virtually the same tropospheric warming. This result indicates that stratospheric processes and vertical resolution due to a higher top are not responsible for the high/low top model difference shown in Figure 3a, and have consequently negligible impact on climate sensitivity. Differences related to model formulation in tropospheric climate processes, such as cloud feedbacks, water vapor, and oceanic (heat transport) processes are therefore implicated.

Figure 3b shows the correlation between the DJF tropical zonal mean temperature change at 300 hPa and SLP, poleward of 20^{o}N. The correlation is negative/positive poleward/equatorward of 60^{o}N. At high latitudes, the correlation is statistically significant. The pattern and sign of the correlation shown in Figure 3b strikingly resembles Figure 2f and suggests that model with larger tropospheric warming (stronger climate sensitivity) tend to simulate stronger extra-tropical SLP changes. Figure 3b therefore provides further support to the interpretation that the difference in the SLP change depicted in Figure 2f is largely due to tropospheric and oceanic processes (directly related to climate sensitivity) rather then the difference in the stratospheric changes between the high and the low top models.

In summary, it is concluded that the high-top minus low-top comparison is not an appropriate subdivision of the CMIP5 model ensemble, if one is searching to identify the impact of the future state of the NH winter polar stratosphere on surface climate within CMIP5.

4.1 An index of polar vortex change

To investigate, whether it is possible to identify the consequences of the future projection of the stratospheric polar vortex within the CMIP5 multi-model set, the CMIP5 models (both high and low top versions) have been divided into two subsets, according to the projected change to the strength of the stratospheric polar vortex. To define the future projection of the stratospheric winds by model, a simple index, hereafter named SUA (S=stratosphere, UA=zonal wind) has been constructed. The SUA index is defined as the zonal mean zonal wind change (2061-2100 minus 1961-2000) at 10 hPa, averaged between 70^{o}-80^{o}N. The 70^{o}-80^{o}N latitudinal band is chosen, because this is where the zonal wind negative change is largest at 10 hPa (see Figure 2a). Hereafter:

- Subset “strong” (labeled CMIP5s) consists of the models with positive SUA index.
- Subset “weak” (labeled CMIP5w) consists of the models with negative SUA index.

So the ‘weak’ subset has a projected response in which the stratospheric winds change shows a dipole structure with weakening/strengthening north/south of 60^{o}N, whereas in the ‘strong’ subset the polar vortex is strengthened up to the pole (as in CMIP3). Figure 4a show the difference CMIP5w minus CMIP5s in the SLP change. This difference clearly shows a quasi-annular pattern, with positive difference over the Arctic, North Atlantic and North European region and negative differences at middle latitudes over the Atlantic basin and South Europe, far East-Asia and Pacific basin. Although a causal relationship cannot be extracted based on Figure 4a, the depicted SLP change difference is consistent with the weakening of the polar stratospheric winds in the CMIP5w models with respect to the CMIP5s. Consequently, Figure 4a can be interpreted as a measure of the uncertainty in surface climate change related to the co-variability of the polar stratospheric wind and the SLP. Over the North Atlantic and European region and the Pacific basin, this uncertainty is of the same order of the CMIP5 projected changes (Figure 2e) and is therefore substantial.

To document if there is a simple relationship between the model spread in the polar stratospheric changes and the high latitude stratospheric climate of the late 20th century, Figure 4b and 4c show scatter plots of the DJF SUA index versus, respectively, the DJF mean and monthly standard deviation of the maximum value of the zonal mean zonal wind at 10 hPa and poleward of 50^{o}N over the period 1961-2000. There appears to be a small but statistically significant correlations between the SUA index and both the zonal wind mean and standard deviation (Table 4, where also JFM values are reported). Most of the models with larger wind mean and std also report more negative SUA indices. High-top models tend to have a larger std and are also in a better agreement with the std derived from ERA40 re-analysis (black lines), while the ERA40 zonal mean wind is located roughly in the middle of the model spread. In JFM, the correlations (Table 4) are slightly larger and also more significant. Although here only a brief analysis of the possible connection between the spread of the modeled stratospheric change and the climatological behavior is presented, overall these results suggest that it can be of interest in a future work to pursue an analysis aimed at characterizing the origin of the model spread including an assessment of the modeled variability (here estimated by the reported monthly std).

4.2 Brewer-Dobson upwelling

Figure 5 shows a comparison of the seasonal evolution and annual mean of the change in total mass upwelling between the so-called 'turnaround' latitudes at 70 hPa i.e. equatorward of the latitudes at which the zonally averaged vertical velocity changes from net upwelling to net downwelling. It is therefore a useful measure of the strength of the Brewer-Dobson (BD) circulation. All models, including the low top versions, agree in the sign of the change, while the high top models show a tendency for a larger increase in strength [*Karpechko and Manzini,* 2012], but the inter-model spread is large. The projected increase in the BD circulation for the end of the 21st century confirms previous multi-models assessments [*Butchart et al.,* 2006; 2010] and provides evidence that stratospheric dynamical processes (e.g., wave drag/forcing) are responsible for the weakening of the high latitude stratospheric winds shown in Figure 2a.

5. CMIP5 projections: Intra-seasonal Changes

Given that the SLP/zonal wind mean changes discussed in Figure 4a are related to other aspects of the tropospheric circulation some of these relationships are here explicitly examined, namely the future projections of atmospheric blocking, tropospheric low-level jets, and storm track activity (section 5.1). We also examine projected changes in the timing of stratospheric final warming (SFW) events [*Black et al.,* 2006] to shed light on the duration into spring of the stratospheric changes reported in Figure 2a and their impacts on the troposphere (section 5.2).

5.1 Blocking, tropospheric low level jets and storminess

Figure 6 shows DJF changes in the latitude-longitude distribution of blocking frequency. Previous studies have shown that most models exhibit unrealistic blocking frequencies, particularly over Europe where large underestimates are common [*D'Andrea et al.,* 1998; *Scaife et al.,* 2010]. Hence the blocking frequency projections must be treated with caution, their value being based on the assumption that model deficiencies play a secondary role, at least in the determining the sign of the changes. Similar to earlier generations of models, blocking biases in CMIP5 models remain large; *Anstey et al.* [2012] give a more detailed analysis of these biases and their relation to low-level jet biases as diagnosed by the Jet Latitude Index (JLI), as well as to stratospheric resolution. Here we define the blocking frequency from daily 500 hPa geopotential height (Z500) using the method by *Scherrer et al.* [2006], which is a two-dimensional (varying in latitude and longitude) generalization of the one-dimensional (varying in longitude only) blocking index by *Tibaldi and Molteni* [1990]. While a variety of different blocking indices have appeared in the literature, the *Scherrer et al.* [2006] index is chosen here because it is straightforward to calculate from a standard CMIP5 model output (daily Z500).

Briefly, the index measures the frequency of large-scale reversals of the meridional gradient of Z500, which are interpreted as the signature of persistent anticyclonic anomalies that would be identified synoptically as blocking. The definition of a blocking event at a given gridpoint, according to this index, is that a reversal of the Z500 meridional gradient equatorward of the gridpoint is simultaneously accompanied by an anomalously strong Z500 meridional gradient (i.e., strong westerlies) poleward of the gridpoint. If these two criteria are satisfied, then an instantaneous blocking event is said to occur. A persistence filter may then be applied to isolate events of long duration. Here the instantaneous frequency is preferred in order to maximize the sample size of events. Applying a five-day persistence filter gives results that are similar but noisier due to the lower frequency of events (not shown) and in general the spatial pattern of blocking frequency has been shown to be relatively insensitive to the particular choice of spatiotemporal filtering that is applied to the instantaneous blocking index [*Davini et al.,* 2012].

Figures 6a and 6b shows that under RCP8.5 forcing conditions, DJF blocking frequency in most regions of the Northern Hemisphere is projected to decrease in the future [*Anstey et al.,* 2012]; the robustness across both model subsets of this general change adds some confidence to the result. The blocking change pattern is broadly similar for CMIP5w and CMIP5s models, but some differences are apparent: CMIP5w models tend to show a weaker blocking decrease over Northern Europe and Greenland than do the CMIP5s models, as indicated by the difference pattern in Figure 6(c). This is broadly consistent with Figure 4(a), which shows increased high-latitude SLP (i.e., a weaker high-latitude SLP decrease) for CMIP5w-CMIP5s. It should be noted that the models used in Figure 6 are a subset of the models used in Figure 4. Figure 6 is limited to those models for which daily geopotential height was available for both historical and RCP 8.5 runs, leaving 13 negative SUA-index and 3 positive SUA-index models. In the previous section it was argued that Figure 4a provides a measure of the uncertainty in future surface climate in the North Atlantic and European region associated with stratospheric changes. In the same way, the CMIP5w-CMIP5s blocking difference in Figure 6c can be interpreted to indicate uncertainty in future blocking frequency in these regions that is associated with stratospheric changes.

Changes in the tropospheric low level jets are diagnosed by means of JLI following *Woollings et al.* [2010]. This index describes the daily variability of the low-level sector-mean zonal wind, where the sector mean is the zonal mean restricted to the longitudes 60°W-0° in the Atlantic basin and 180°W-120°W in the Pacific basin. The JLI is defined as the latitude, within the regions 15°N-75°N for the Atlantic and 15°-65° for the Pacific, where the maximum of the sector-mean zonal wind occurs on each day. The 850 hPa zonal wind is used, and a 5-day running mean followed by interpolation onto a standard 2.5°x2.5° grid are performed before computing the JLI. Only models for which daily zonal wind is available for both historical and RCP8.5 experiments are used, yielding a subset of 15 models out of the 22 models listed in Table 1. Figure 7 shows that modeled JLI distributions are generally more sharply peaked than ERA-40, indicating too little variability of jet position in the models. In the Atlantic basin, the multi-model mean fails to capture the extent of JLI distribution trimodality seen in the reanalyses, although a small number of models do exhibit distinctly trimodal distributions (not shown). Virtually all models, however, underestimate the magnitude of the poleward Atlantic JLI peak.

In the future RCP8.5 scenario, Figure 7a (thin lines) shows that the Atlantic jet becomes increasingly likely to be found at the central JLI peak rather than the equatorward or poleward peaks. This change is more pronounced for CMIP5s than CMIP5w models. The fact that the CMIP5w models show a weaker overall blocking frequency decrease (Figure 6c) is consistent with the trend towards more central JLI being weaker for the CMIP5w models. Studies of reanalyses data show that high-latitude blocking favours equatorward jet displacement [*Woolings et al.,* 2010; *Davini et al.,* 2012]. Hence the negative trend in high-latitude Atlantic blocking is consistent with decreased occurrence of the equatorward Atlantic jet position, and this also occurs more prominently for the CMIP5s models, concomitantly with a stronger decrease of high-latitude Atlantic blocking.

In the Pacific, Figure 7(b) shows that the jet shifts poleward in the future, with this shift being slightly more pronounced for the CMIP5s (positive SUA index) models. The weaker association between the JLI and stratospheric polar wind changes may be due to the Pacific jet being located further equatorward and having more of the character of a subtropical jet (in contrast to the Atlantic eddy-driven jet, which is often separated from the subtropical jet). Similarly to the Atlantic, decreased equatorward JLI in the Pacific is accompanied by negative blocking frequency changes at high latitudes.

Figures 8a and 8b shows the projection to the end of the 21st century of storm track activity, given by the 2-6 days bandpass filtered SLP standard deviation [*Ulbrich et al.,* 2008], separated according to the stratospheric polar wind change, while Figure 8c shows the CMIP5w-CMIP5s difference in storm track activity change. As in the case of the blocking frequency, the change in storm track activity is broadly similar for the CMIP5w and CMIP5s models, but some differences are apparent. Specifically, the difference CMIP5w-CMIP5s in the storm track activity change shows a smaller increase in storm track activity in the North-Atlantic and North Pacific regions in CMIP5w with respect to CMIP5s (Figure 8c). Therefore, changes in storm track activity accompany the difference in mean SLP change (Figure 4a) and are also consistent with the smaller decrease in blocking (Figure 6c). Although it is of interest to note the strong association between the state of the stratospheric vortex and the storminess, it must be kept in mind that tropospheric storm track activity is strongly influenced by tropospheric and oceanic processes affecting the surface atmospheric baroclinicity [*Wollings et al.* 2012].

5.2 Stratospheric final warming

The tropospheric impact of stratospheric final warming (SFW) events was first studied in *Black et al.* [2006]. They found that SFW events (a) sharply weaken the high latitude westerlies in comparison to climatological trend values while (b) providing a pattern of height rises (falls) over polar latitudes (oceanic mid to high latitudes). The statistical behavior of stratospheric final warming events in historical simulations of CMIP5 models is examined by *Charlton-Perez et al.* [2012]. The main result is that boreal SFW events are typically delayed by an average of about 2 weeks in CMIP5 simulations compared to parallel results derived from reanalyses.

Here we extend the statistical analyses of *Charlton-Perez et al.* [2012] to identify the ensemble average tropospheric impact of SFW events in both historical and RCP8.5 CMIP5 simulations. Boreal SFW onset dates are identified using the methods of *Black et al.* [2006]. Circulation anomalies are taken as deviations from the first six Fourier harmonics of a repeating annual cycle (itself obtained by concatenating long-term daily averages for each calendar day). Finally, we assess the tropospheric impact of SFW events by considering the composite (among all SFW events for each simulation) circulation anomaly difference occurring during a 20-day period surrounding SFW onset. For each model configuration studied we analyze one member of the historical simulation ensemble (Table 3), since the results do not vary appreciably among the ensemble members. The results for the historical simulation ensembles are displayed in Figure 9. The composite difference in zonal-mean zonal wind anomalies illustrates that CMIP5 models faithfully represent the coupled stratosphere-troposphere signature identified in *Black et al*. [2006]. Specifically, SFW events are associated with a statistically significant zonal deceleration /acceleration within sub-polar /low-middle latitudes (compare with Figure 3 of *Black et al.* [2006]) in the multi-model ensembles. The zonal wind change is linked to a parallel north-south dipole in sea level pressure anomaly change with significant pressure increases /decreases at polar /middle latitudes. Similar analyses of surface air temperature reveal that SFW events are linked to significant polar warming (particularly in the western hemisphere) and cooling over northernmost Eurasia. This pattern is consistent with the idea that SFW events help to facilitate spring onset within portions of the Arctic [*Black et al.,* 2006].

We have also performed parallel analyses of RCP8.5 model simulations. We find that (a) there is no significant change observed in the average timing of SFW events and (b) the stratospheric and tropospheric circulation anomaly change patterns associated with SFW events are not statistically distinct from those found for the historical model ensembles (i.e., the results closely resemble those presented in Figure 9 and, for brevity, are not shown). To summarize our results: While CMIP5 models are able to represent the salient characteristics of the tropospheric response to SFW events, there is no discernible change in either the behavior of SFW events or their tropospheric impact between the historical and RCP8.5 model ensembles.

Concerning the timing of the SFW and the projection of the mean stratospheric zonal wind change: (a) there does not appear to be any consistent relationship between SFW timing and either the SUA index or the location of the model top and (b) there are substantial changes observed for individual models, ranging from -20 days (e.g., CNRM-CM5) to +13 days (MIROC-ESM-CHEM and CSIRO-MK33-6-0). We therefore conclude the stratospheric changes reported in Figure 2a do not extend into the spring season, at least in such a way to affect the timing of the SFW events.

6. Discussion and Conclusion

Stratospheric changes and their potential associated surface signatures in the CMIP5 ensemble of models have been assessed for the period 1961-2100, focusing on the NH winter stratosphere-troposphere climate, when the stratosphere-troposphere dynamical coupling is most active. A CMIP5 and CMIP3 comparison has also been addressed. The main findings are summarized here:

(1) The NH stratospheric zonal wind projected changes to the end of the 21^{st} century are likely to be characterized by a dipolar pattern, with stronger winds at low latitudes, further upward extension of the well known upward (and poleward) shift and strengthening of the subtropical tropospheric jet, and weaker winds at high latitudes. Comparison with CMIP3 for the 1% per year CO_2 increase experiment has shown that this dipolar pattern is a novel feature of the CMIP5 ensemble of models

relative to the CMIP3 ensemble of models. On the basis of the projected increase in the BD circulation, reported previously [*Butchart and Scaife*, 2001] and also found here in the CMIP5 model ensembles, and knowledge from previous literature [*Sigmond et al.,* 2004; *Bell,* 2009], the stratospheric polar wind change (the weakening) is interpreted as a remote dynamical response of the stratosphere to changes in tropospheric and oceanic processes as a result of greenhouse gas forcing. Although changes in stratospheric wave drag and/or forcing are obviously implicated in a remote stratospheric dynamical response, open and left for future investigation are the specific mechanisms linking the troposphere to stratosphere dynamical response and their relative role. In addition, the spread of the modeled stratospheric polar changes within the CMIP5 models calls for a better understanding of the relative role and interdependence of stratospheric dynamical processes and other factors (such as climate sensitivity, sea surface temperature and/or ozone changes) in leading to the reported stratospheric mean changes.

(2) The height of the model top in the CMIP5 model ensembles is not a good predictor of high latitude stratospheric change and consequently of the impact of the future projection of the NH winter polar stratosphere on surface climate. The majority of high-top models report a larger tropospheric warming than the low top models. Results from three high/low-top controlled experiments indicate that for these high/low-top model pairs the tropospheric warming is comparable. It is therefore reasonable to assert that stratospheric processes and vertical resolution are not implicated in the difference in the tropospheric warming of the high/low-top models. The CMIP5 high and low top inter-comparison suggests that either the CMIP5 set of opportunity does not guarantee that uncertainty in model formulations are

appropriately considered (e.g., too few models, models sharing parameterizations and/or components), or that uncertainty in modeling the tropospheric processes is so large that it overwhelms any improvement introduced by the addition of stratospheric processes, or both.

(3) By sub-dividing the CMIP5 model set by the change in the strength of the stratospheric polar vortex (SUA index), co-variability of the stratospheric polar winds with mean SLP and in intra-seasonal tropospheric processes is revealed. Namely, high latitude stratospheric wind weakening is found to coexist with smaller high-latitude mean SLP decrease, smaller decrease in high-latitude blocking frequency and JLI changes and smaller increase in storm track activity in the North-Atlantic and North Pacific regions. It is therefore concluded that a relatively large uncertainty in surface climate change related to this co-variability is present within the whole CMIP5 ensemble of models. A causal relationship cannot be extracted by the analysis presented. Nevertheless, the fact that the link between weakening of the stratospheric winds and smaller high-latitude mean SLP decrease found here is consistent with the results by *Scaife et al.* [2012] and *Karpechko and Manzini* [2012], obtained by means of high/low top controlled experiments, suggests that stratosphere to troposphere coupling is implicated in the CMIP5 results. Further experimentations by means of specifically designed simulations to further corroborate the role of the stratosphere are nevertheless called for.

(4) The whole CMIP5 ensemble of models is capable to represent the salient characteristics of the tropospheric response to stratospheric final warming. The analysis of the projection to the end of the 21st century following the RCP8.5

scenarios has shown that there is no discernible change in either the behavior of SFW events or their tropospheric impact between the historical and RCP8.5 model ensembles. In addition, there does not appear to be any consistent relationship between SFW timing and either the SUA index or the location of the model top. The reported stratospheric polar wind changes therefore do not extend into the spring season, at least in such a way to affect the timing of the SFW events.

To test the sensitivity of the zonal wind and temperature changes shown in Figure 2, to 20th century ozone depletion, Figure 2 has been calculated also for 2061-2100 RCP8.5 minus 1861-1900 historical, given that after 2050, stratospheric ozone is projected to recover in the RCP8.5 scenario, and the NH stratospheric ozone radiative forcing returns to that of the 19th century level [*Cionni et al.,* 2011]. The results shown in Figure 2 are fully reproduced for the 2061-2100 RCP8.5 minus 1861-1900 historical averaged changes, with slightly larger responses (in magnitude). It is therefore concluded, that ozone is not the primarily driver of the stratospheric changes shown in Figure 2. Nevertheless, it is noted that at the end of the 21st Century upper stratospheric ozone will be expected to be larger than at the end of the 19th Century, due to the CO_2 cooling of the middle atmosphere. This is a feature included in the CMIP5 ozone dataset [*Cionni et al.,* 2011]. The reported stratospheric changes are therefore also not an artificial response to an increase in CO_2 that does not take into account the ozone-temperature feedback in the middle atmosphere, and hence artificially cold stratopause temperature [*Jonsson et al.,* 2004].

In summary, on the basis of the present analysis and the *Charlton-Perez et al.* [2012] assessment, it is concluded that it is the improvement in the stratospheric mean state in both high top and low top CMIP5 models relative to the CMIP3 models, that most likely explains the CMIP5 projected weakening of the polar stratospheric zonal winds, which was absent in the CMIP3 multi-model averages. Given that the assessment by *Charlton-Perez et al.* [2012] has shown that the high and low-top models have comparable stratospheric mean flow performance but different stratospheric variability at all scales (with the low-top model variability comparable to that of the CMIP3 models), it is plausible to ask what is the role of the improved stratospheric variability of the high-top models in leading to the reported stratospheric changes. Knowledge of how sub-grid scale processes, such as dissipation and gravity wave effects, are treated in the individual models and to what extent the sub-grid scale schemes may potentially correctly compensate for deficiencies in variability in the CMIP5 low-top models, is needed to answer this question, but this is clearly outside the scope of this multi-model assessment. This interesting question on the interaction between resolved and parameterized dynamics is therefore left open for future investigations.

Acknowledgements

We acknowledge the World Climate Research Programme's Working Group on Coupled Modelling, which is responsible for CMIP, and we thank the climate modeling groups for producing and making available their model output. For CMIP the U.S. Department of Energy's Program for Climate Model Diagnosis and Intercomparison provides coordinating support and led development of software infrastructure in partnership with the Global Organization for Earth System Science Portals. This work was partially funded by the European Commission's 7th

Framework Programme, under GA # 226520, COMBINE project. AAS was supported by the Joint DECC/Defra Met Office Hadley Centre Climate Programme (GA01101). MPB was funded by NSF under the US CLIVAR program and the Office of Polar Programs. The research efforts of RXB, BAM & Y-YL were supported by the Office of Science (BER) of the U.S. Department of Energy and by the National Science Foundation Grant, ARC-1107384. AYK was funded by the Finnish Academy (the project CACSI and personal postdoctoral project). JA and LJG were funded by the UK Natural Environment Research Council (NERC) and National Centre for Atmospheric Science (NCAS).

References

Andrews, D. G., J. R. Holton, and C. B. Leovy (1987), Middle Atmospheric Dynamics, 489pp., Academic, San Diego, CA.

Anstey, J. A., P. Davini, L. J. Gray, and T. J. Woollings, et al (2012), Multi-model analysis of Northern Hemipshere winter blocking and tropospheric jet variability, in preparation.

Baldwin, M. P., and T. J. Dunkerton (2001), Stratospheric harbingers of anomalous weather regimes, Science, 294, 581–584.

Bell, C.J. (2009), The Role of Stratospheric Variability in Climate, PhD Thesis, Reading University, UK.

Bell, C. J., L. J. Gray, and J. Kettleborough (2010), Changes in Northern Hemisphere stratospheric variability under increased CO2 concentrations, Q. J. R. Meteorol. Soc., 136:1181–1190.

Black, R. X., B. A. McDaniel, and W. A. Robinson (2006), Stratosphere-Troposphere coupling during spring onset, J. Climate, 19, 4891-4901.

Butchart, N., A. A. Scaife (2001) Removal of chlorofluorocarbons by increased mass exchange between the stratosphere and troposphere in a changing climate. Nature 410:799–802

Butchart, N., et al. (2006), Simulations of anthropogenic change in the strength of the Brewer-Dobson circulation, Clim. Dyn., 27, 727–741, doi:10.1007/s00382-006-0162-4.

Butchart, N., et al. (2011), Multimodel climate and variability of the stratosphere, J. Geophys. Res., 116, D05102, doi:10.1029/2010JD014995.

Calvo, N. and R. R. Garcia (2009), Wave forcing of the Tropical Upwelling in the Lower Stratosphere under Increasing Concentrations of Greenhouse Gases, J. Atm. Sci. 66, 3184-3196, doi:10.1175/2009JAS3085.1

Charlton-Perez, A., et al. (2012), Mean Climate and Variability of the Stratosphere in the CMIP5 models, J. Geophys. Res. (submitted)

Cionni, I., et al. (2011), Ozone database in support of CMIP5 simulations: results and corresponding radiative forcing, Atmos. Chem. Phys., 11, 11267–11292. doi:10.5194/ acp-11-11267-2011.

D'Andrea, F., et al. (1998), Northern Hemisphere atmospheric blocking as simulated by 15 atmospheric general circulation models in the period 1979-1988, Clim. Dyn., 14, 385-407.

Davini, P., C. Cagnazzo, S. Gualdi, and A. Navarra (2012), Bidimensional diagnostics, variability and trends of Northern Hemisphere Blocking, J. Clim., doi:10.1175/JCLI-D-12-00032.1, in press.

Garcia, R.R. and W.J. Randel (2008), Acceleration of the Brewer-Dobson circulation due to increases in greenhouse gases, J. Atm. Sci., 65, 2731-2739.

Gettelman, A., and Q. Fu (2008), Observed and Simulated Upper-Tropospheric Water Vapor Feedback, J. Clim., 21, 3282-3289.

Hardiman, S. C., N. Butchart, T. J. Hinton, S. M. Osprey, and L. J. Gray (2012), The effect of a well resolved stratosphere on surface climate: Differences between CMIP5 simulations with high and low top versions of the Met Office climate model, J. Clim. (in press)

IPCC, 2007: Climate Change 2007: The Physical Science Basis. Contribution of Working Group I to the Fourth Assessment Report of the Intergovernmental Panel on

Climate Change [Solomon, S., D. Qin, M. Manning, Z. Chen, M. Marquis, K.B. Averyt, M. Tignor and H.L. Miller (eds.)]. Cambridge University Press, Cambridge, United Kingdom and New York, NY, USA, 996 pp.

Jonsson, A. I., J. de Grandpré, V. I. Fomichev, J. C. McConnell, and S. R. Beagley (2004), Doubled CO_2-induced cooling in the middle atmosphere: Photochemical analysis of the ozone radiative feedback, J. Geophys. Res., 109, D24103, doi:10.1029/2004JD005093, 2004

Karpechko, A. Y. and E. Manzini (2012), Stratospheric influence on tropospheric climate change in the Northern Hemisphere, J. Geophys. Res., 117, D05133, doi:10.1029/2011JD017036.

McLandress, C., and T. G. Shepherd (2009), Impact of climate change on stratospheric sudden warmings as simulated by the Canadian Middle Atmosphere Model, J. Clim., 22, 5449–5463.

Scaife A. T. Woollings, J. Knight, G. Martin, and T. Hinton (2010), Atmospheric blocking and mean biases in climate models, J. Climate, 23, 6143-6152.

Scaife et al. (2012), Climate change projections and stratosphere–troposphere interaction, Climate Dyn., doi: 10.1007/s00382-011-1080-7.

Scherrer, S., M. Croci-Maspoli, C. Schwierz}, and C. Appenzeller (2006), Two-dimensional indices of atmospheric blocking and their statistical relationship with winter climate patterns in the Euro-Atlantic region, Int. J. Climatol., 26, 233-249.

Shepherd, T.G. and C. McLandress (2011), A Robust Mechanism for Strengthening of the Brewer–Dobson Circulation in Response to Climate Change: Critical-Layer Control of Subtropical Wave Breaking, J. Atmos. Sci., 68, 784-797.

Shindell, D. T., R. L. Miller, G. Schmidt, and L. Pandolfo (1999), Simula- tion of the Arctic Oscillation trend by greenhouse forcing of a stratospheric model, Nature, 399, 452–455, doi:10.1038/20905.

Sigmond, M., and J. F. Scinocca (2010), The influence of the basic state on the Northern Hemisphere circulation response to climate change, J. Clim., 23, 1434–1446, doi:10.1175/2009JCLI3167.1.

Sigmond, M., P. C. Siegmund, E. Manzini, and H. Kelder (2004), A simulation of the separate climate effects of middle atmospheric and tropospheric CO2 doubling, J. Clim., 17, 2352–2367.

Solomon, S., et al (2007), Technical Summary. In: Climate Change 2007: The Physical Science Basis. Contribution of Working Group I to the Fourth Assessment Report of the Intergovernmental Panel on Climate Change [Solomon, S., D. Qin, M. Manning, Z. Chen, M. Marquis, K.B. Averyt, M. Tignor and H.L. Miller (eds.)]. Cambridge University Press, Cambridge, United Kingdom and New York, NY, USA.

Tibaldi, S. and F. Molteni (1990), On the operational predictability of blocking, Tellus, 42A, 343-365.

Ulbrich, U., J. G. Pinto, H. Kupfer, G. C. Leckebusch, T. Spangehl, and M. Reyers (2008), Changing Northern Hemisphere Storm Tracks in an Ensemble of IPCC Climate Change Simulations, J. Climate, 21, 1669–1679, doi:10.1175/ 2007JCLI1992.1.

van Vuuren, D. P., J. A. Edmonds, M. Kainuma, K. Riahi, and J. Weyant (2011), A special issue on the RCPs, Climatic Change, 109, DOI 10.1007/s10584-011-0157-y

Woollings, T., A. Hannachi, and B. Hoskins (2010), Variability of the North Atlantic eddy-driven jet stream, Quart. J. Roy. Meteor. Soc., 136, 856-868.

Woollings, T., J. M. Gregory, J. G. Pinto, M. Reyers, and D. J. Brayshaw (2012), Response of the North Atlantic storm track to climate change shaped by ocean–atmosphere coupling, Nature Geoscience, 5, 313–317, doi:10.1038/ngeo1438.

Figure Captions

Figure 1: 1pctCO2 experiments: DJF change (101 to 140 average) minus (1 to 40 average). Zonal mean zonal wind (ms^{-1}): (a) CMIP5 and (b) CMIP3 multi-model ensembles. CMIP5 minus CMIP3 difference in the change, for (c) zonal mean zonal wind (ms^{-1}) and (d) zonal mean temperature (K). PSL (hPa): (e) CMIP5 multi-model ensemble. (f) CMIP5 minus CMIP3 difference in the change. Shading: In panels (a), (b), (e) Dark (light) shadings mark inter-model sign consistence at the 90% (66%) level. In panels (c), (d), and (f): Dark (light) shadings mark 2-tailed t-test statistical significance difference in the responses with $p < 0.05$ (<0.1).

Figure 2: DJF change (2061-2100 rcp8.5 minus 1961-2000 historical). Zonal mean zonal wind (ms^{-1}): (a) CMIP5 multi-model ensemble and (b) CMIP5 high-top multi-model minus CMIP5 low-top multi-model difference in the change. Zonal mean temperature (K): (c) CMIP5 multi-model ensemble and (d) CMIP5 high-top multi-model minus CMIP5 low-top multi-model difference in the change. PSL (hPa): (e) CMIP5 multi-model ensemble. (f) CMIP5 high-top multi-model minus CMIP5 low-top multi-model difference in the change. Shading: In panels (a), (c), (e) Dark (light) shadings mark inter-model sign consistence at the 90% (66%) level. In panels (b), (d), and (f): Dark (light) shadings mark 2-tailed t-test statistical significance difference in the responses with $p < 0.05$ (<0.1).

Figure 3: CMIP5 multi-model ensemble. (a) Scatter plot of the annual, tropical (30^oS-30^oN) and zonal mean temperature change (2061-2100 rcp8.5 minus 1961-2000 historical) at 300 hPa versus its respective mean change at 850 hPa, by model. Each

signature represents a model, high-top models in read and low-top models in blue. One model (green) is intermediate. High/low-top model "pairs" (see text) shown by squares. (b) Correlation of the DJF tropical (30^oS-30^oN, 300 hPa) zonal mean temperature change with SLP, poleward of 20^oN. Dark (light) shadings mark 2-tailed t-test statistical significance of correlation coefficient with $p < 0.05$ (<0.1).

Figure 4: (a) DJF SLP (hPa) change (2061-2100 rcp8.5 minus 1961-2000 historical): Difference in the change composited with respect to the sign of the projected stratospheric zonal mean zonal wind change by the CMIP5 models (SUA index, see text), negative SUA index (CMIP5w) model subset average minus positive SUA index (CMIP5s) model subset. Dark (light) shadings mark student t-test statistical significance difference in the responses with $p < 0.05$ (<0.1). (b) Scatter plot of zonal mean zonal wind change (2061-2100 rcp8.5 minus 1961-2000 historical) at 10 hPa, averaged between 70-80 N (SUA Index) versus (1961-2000) zonal mean zonal wind maximum at 10 hPa, poleward of 50^oN, by model. (c) as (b) but versus the (1961-2000) monthly (D, F, J) zonal mean zonal wind standard deviation at the wind max location. Each signature represents a model, high-top models in read and low-top models in blue. One model (green) is intermediate. Black lines in (b) and (c) are ERA40 (1960-1999) DJF zonal mean zonal wind maximum at 10 hPa and poleward of 50^oN and monthly (D, F, J) zonal mean zonal wind standard deviation at the wind max location, respectively. In (b) and (c), red/blue/green signatures mark high/low /intermediate top models.

Figure 5: CMIP5 multi-model ensemble. Change (2060-2100 rcp8.5 minus 1960-2000 historical) in total mass upwelling (10^9 kgs^{-1}) between turn around latitudes at

70 hPa. CMIP5 high-top models in red and CMIP5 low-top models in blue. (a) seasonal cycle from July to June. (b) Annual mean by model and by high/low top model subsets.

Figure 6: Change (2060-2100 RCP8.5 minus 1960-2000 historical) DJF blocking frequency for (a) CMIP5w (negative SUA index) model subset, (b) CMIP5s (positive SUA index) model subset; and (c) their difference. The blocking frequency is based on 500 hPa geopotential height and is given as the percentage of blocked days, with red/blue contours indicating positive/negative changes (a and b) and difference in the changes (c). Stippling mark 2-tailed t-test statistical significance with $p < 0.05$. For context the thick black line in shows the 1% contour of the ERA-40 climatological DJF blocking frequency.

Figure 7: DJF Jet Latitude Index distribution for the (a) Atlantic and (b) Pacific sectors. Thick solid lines show ensemble-mean distributions for the 1961-2000 period of the historical runs for CMIP5 models (black), CMIP5w (negative SUA index, red) model subset and CMIP5s (positive SUA index, blue) model subset. Thin solid lines show the respective changes (2061-2100 RCP8.5 minus 1961-2000 historical) in distributions, and filled circles mark 2-tailed t-test statistical significance with $p < 0.05$. ERA-40 1961-2000 JLI distributions (thick dashed black lines) are shown for comparison. All distributions are plotted as kernel estimates using a Gaussian kernel with standard deviation 2.5^{o} (the spacing of the latitudinal grid on which the JLI is defined).

Figure 8: Change (2060-2100 RCP8.5 minus 1960-2000 historical) DJF storm track activity for (a) CMIP5w (negative SUA index) model subset, (b) CMIP5s (positive SUA index) model subset; and (c) their difference. Storm track activity is given by the 2--6 days bandpass filter standard deviation of mean SLP, in units of 1/10 of hPa. Red/blue contours indicating positive/negative changes (a and b) and difference in the changes (c). Stippling mark t-test statistical significance with $p < 0.05$. For context, in (a) and (b) the contours show the multi--model mean values in the historical simulations (contour interval: 1 hPa).

Figure 9: Differences in circulation anomalies occurring during a 20-day period surrounding NH SFW events as represented in the 1961-2000 averaged historical ensemble of CMIP5 models. (a) zonal mean zonal wind (ms^{-1}); (b) SLP (hPa); (c) surface air temperature (K). Blue and yellow contours are displayed to enclose regions in which the anomaly difference is statistically significant according to a 2-sided t-test.

Table 1: Models used in the CMIP3 & CMIP5 comparison (1%CO_2 experiments**)**

Institution	***CMIP3 MODEL***	***CMIP5 MODEL***
CCCMA	cccma_cgcm3_1	CanESM2
CNRM-CERFACS	cnrm_cm3	CNRM-CM5
NOAA GFDL	gfdl_cm2_0	
NASA GISS	giss_model_e_r	
INGV	ingv_echam4	
INM	inmcm3_0	
IPSL	ipsl_cm4	IPSL-CM5A-LR
MIROC	miroc3_2_medres	MIROC5
FUB	miub_echo_g	
MRI	mri_cgcm2_3_2a	MRI-CGCM3
NCAR	ncar_ccsm3_0	
PCMDI	ncar_pcm1	
MPI-M		MPI-ESM-LR
MPI-M		MPI-ESM-P
BCC CMA		NorESM1-ME

Table 2: CMIP5 models used in projections (rcp8.5 and historical experiments)

Institution	**Model**	**Top**	**Levels**	**Subset**
CMCC	CMCC-CESM	0.01 hPa	39	HIGH TOP
	CMCC-CMS	0.01 hPa	95	HIGH TOP
	EC-EARTH-HIGH			HIGH TOP
NOAA GFDL	GFDL-CM3	0.01 hPa	48	HIGH TOP
NASA GISS	GISS-E2-R	0.1 hPa	40	HIGH TOP
MOHC	HadGEM2-CC	85 km	60	HIGH TOP
IPSL	IPSL-CM5A-LR	0.04 hPa	39	HIGH TOP
	IPSL-CM5A-MR	0.04 hPa	39	HIGH TOP
MIROC	MIROC-ESM-CHEM	0.0036 hPa	80	HIGH TOP
	MIROC-ESM	0.0036 hPa	80	HIGH TOP
MPI-M	MPI-ESM-LR	0.01 hPa	47	HIGH TOP
	MPI-ESM-MR	0.01 hPa	95	HIGH TOP
MRI	MRI-CGCM3	0.01 hPa	48	HIGH TOP
NCAR	WACCM4			HIGH TOP
CCCMA	CanESM2	1 hPa	35	-
BCC CMA	bcc-csm1-1	2.917 hPa	26	LOW TOP
NCAR	CCSM4	2.194 hPa	27	LOW TOP
CMCC	CMCC-CESM-LOW	10 hPa	19	LOW TOP
CNRM-CERFACS	CNRM-CM5	10 hPa	31	LOW TOP
CSIRO-QCCCE	CSIRO-Mk3-6-0	4.52 hPa	18	LOW TOP
	EC-EARTH-LOW			
NOAA GFDL	GFDL-ESM2M	3 hPa	24	LOW TOP
MOHC	HadGEM2-ES	40 km	38	LOW TOP
INM	inmcm4	10 hPa	21	LOW TOP
MIROC	MIROC5	3 hPa	56	LOW TOP

NCC	NorESM1-M	3.54 hPa	26	LOW TOP

Table 3: CMIP5 models by diagnostic: Number of realizations by model.

	figs 2,3b,4			fig 3a	fig 5	fig 6	fig7	fig8	fig9
Model	**psl**	**ua**	**ta**	**ta**	**mass flux**				
CMCC-CESM	1	1	1	1	1	1	1		
CMCC-CMS	1	1	1		1	1	1	1	
EC-EARTH-HIGH	1	1	1	1					
GFDL-CM3				1	1				
GISS-E2-R	1	1	1	1	1				
HadGEM2-CC	3	3	1	1	1	3	3	1	1
IPSL-CM5A-LR	4	4	1	1		5	5	1	1
IPSL-CM5A-MR	1	1	1	1		1	1	1	1
MIROC-ESM-CHEM	1	1	1	1	1	1	1	1	1
MIROC-ESM	1	1	1	1	1			1	
MPI-ESM-LR	2	2	1	1	1	3	3		1
MPI-ESM-MR	1	1	1			3			
MRI-CGCM3	1	1	1	1	1	1	1		1
WACCM4					1				
CanESM2	5	5	1	1		5	5	1	
bcc-csm1-1	1	1	1	1		1	1	1	
CCSM4	5	5	1	1				1	
CMCC-CESM-LOW	1	1	1	1		1	1		
CNRM-CM5	3	3	1	1				1	1
CSIRO-Mk3-6-0	1	1	1	1				1	1
EC-EARTH-LOW	1	1	1	1	1	1		1	
GFDL-ESM2M				1			1		1
HadGEM2-ES	3	3	1	1	1	4	1	1	
inmcm4	1	1	1	1	1			1	1
MIROC5	1	1	1	1		4	4	1	1
NorESM1-M	1	1	1	1		3	3		

Table 4: Correlation (significance) between the SUA index and zonal mean zonal wind max and std (historical, 1961-200)

	DJF	**JFM**
mean max	-0.39 (p=0.07)	-0.51 (p=0.01)
std	-0.45 (p=0.03)	-0.52 (p=0.01)

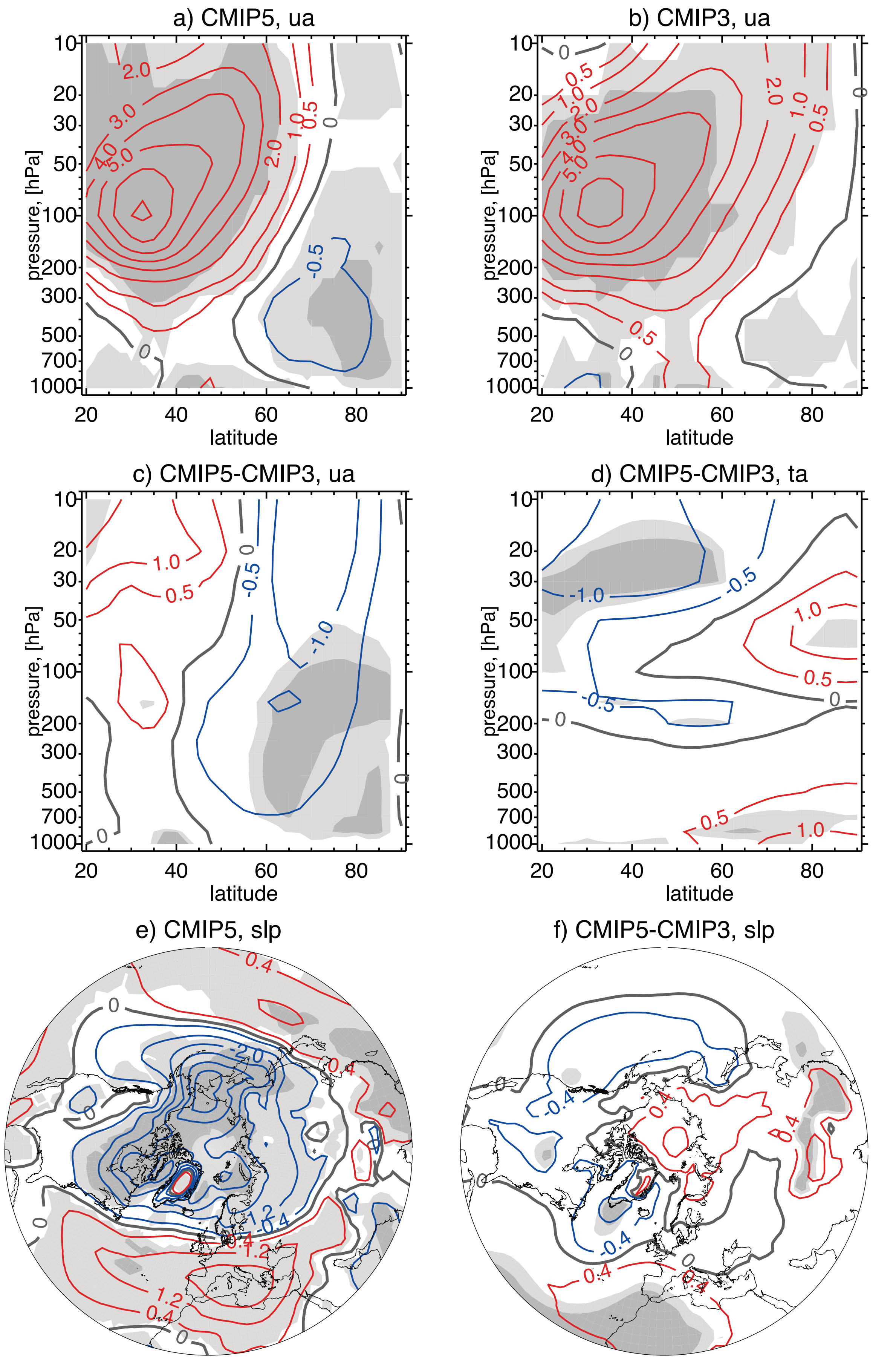

a) CMIP5, ua
b) CMIP3, ua
c) CMIP5-CMIP3, ua
d) CMIP5-CMIP3, ta
e) CMIP5, slp
f) CMIP5-CMIP3, slp
pressure, [hPa]
latitude
10
20
30
50
100
200
300
500
700
1000
20
40
60
80

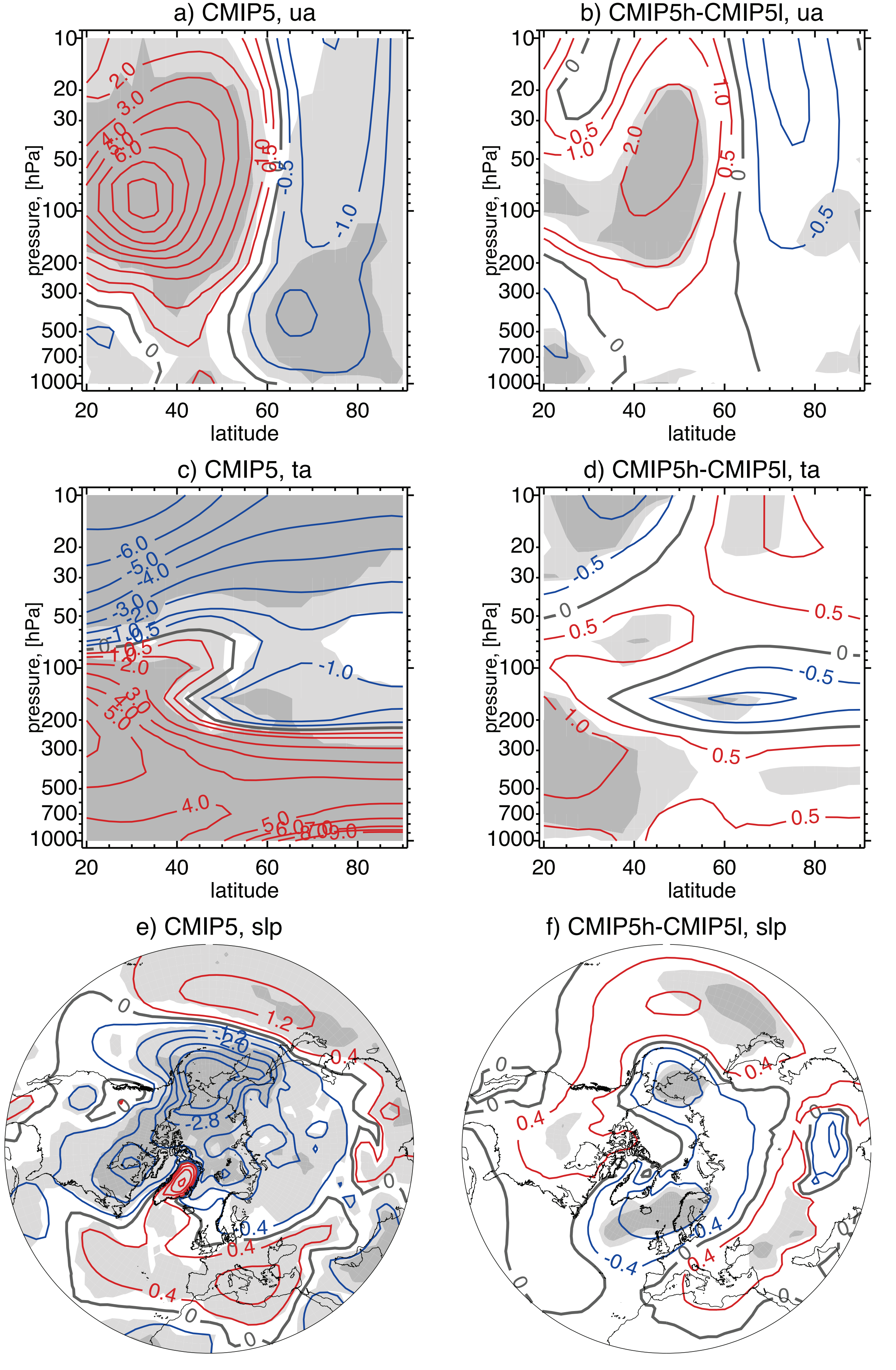
a) CMIP5, ua
b) CMIP5h-CMIP5l, ua
c) CMIP5, ta
d) CMIP5h-CMIP5l, ta
e) CMIP5, slp
f) CMIP5h-CMIP5l, slp
pressure, [hPa]
latitude

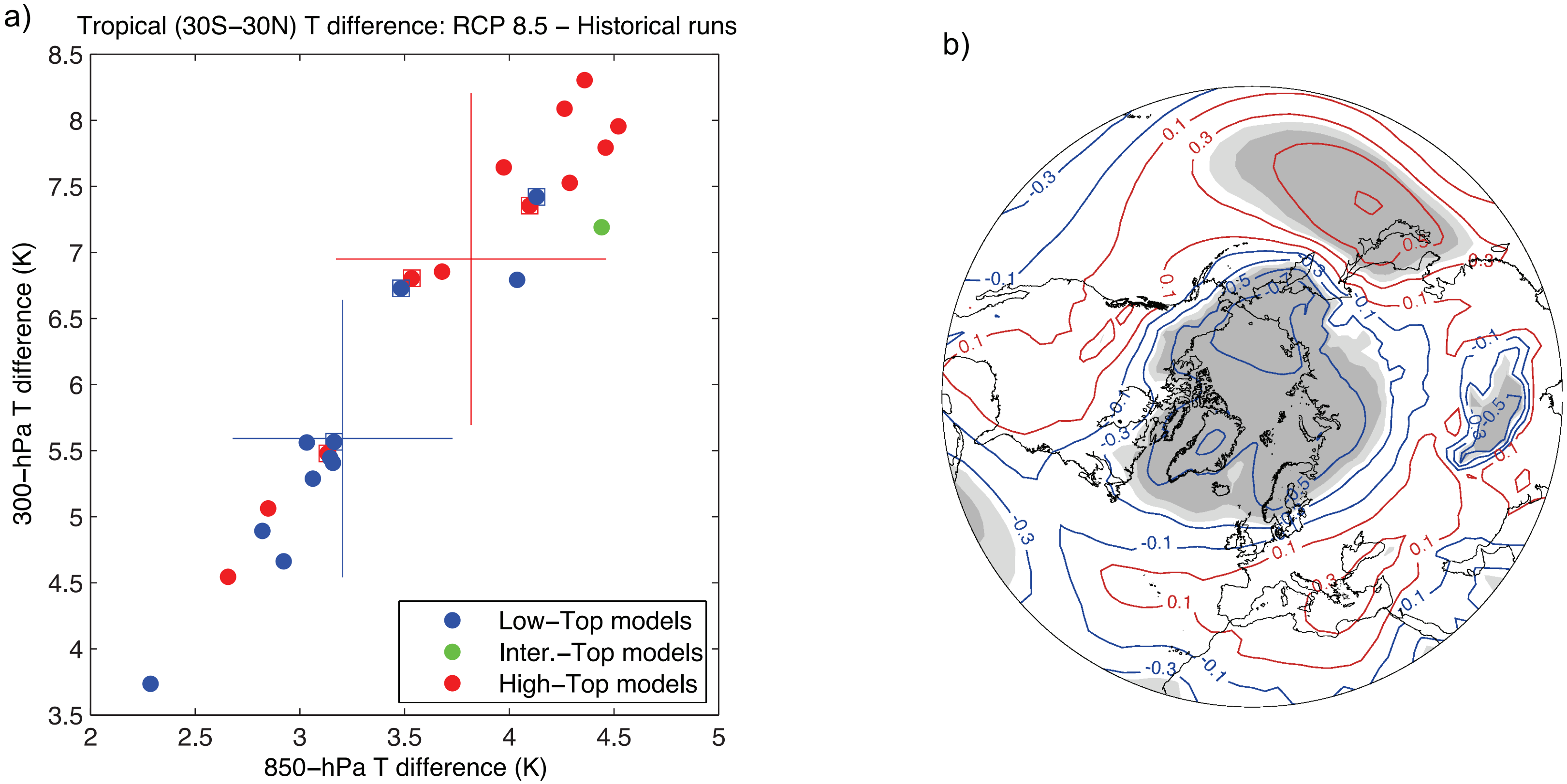
a)
Tropical (30S–30N) T difference: RCP 8.5 – Historical runs
300–hPa T difference (K)
850–hPa T difference (K)
8.5
8
7.5
7
6.5
6
5.5
5
4.5
4
3.5
2
2.5
3
3.5
4
4.5
5
Low–Top models
Inter.–Top models
High–Top models
b)

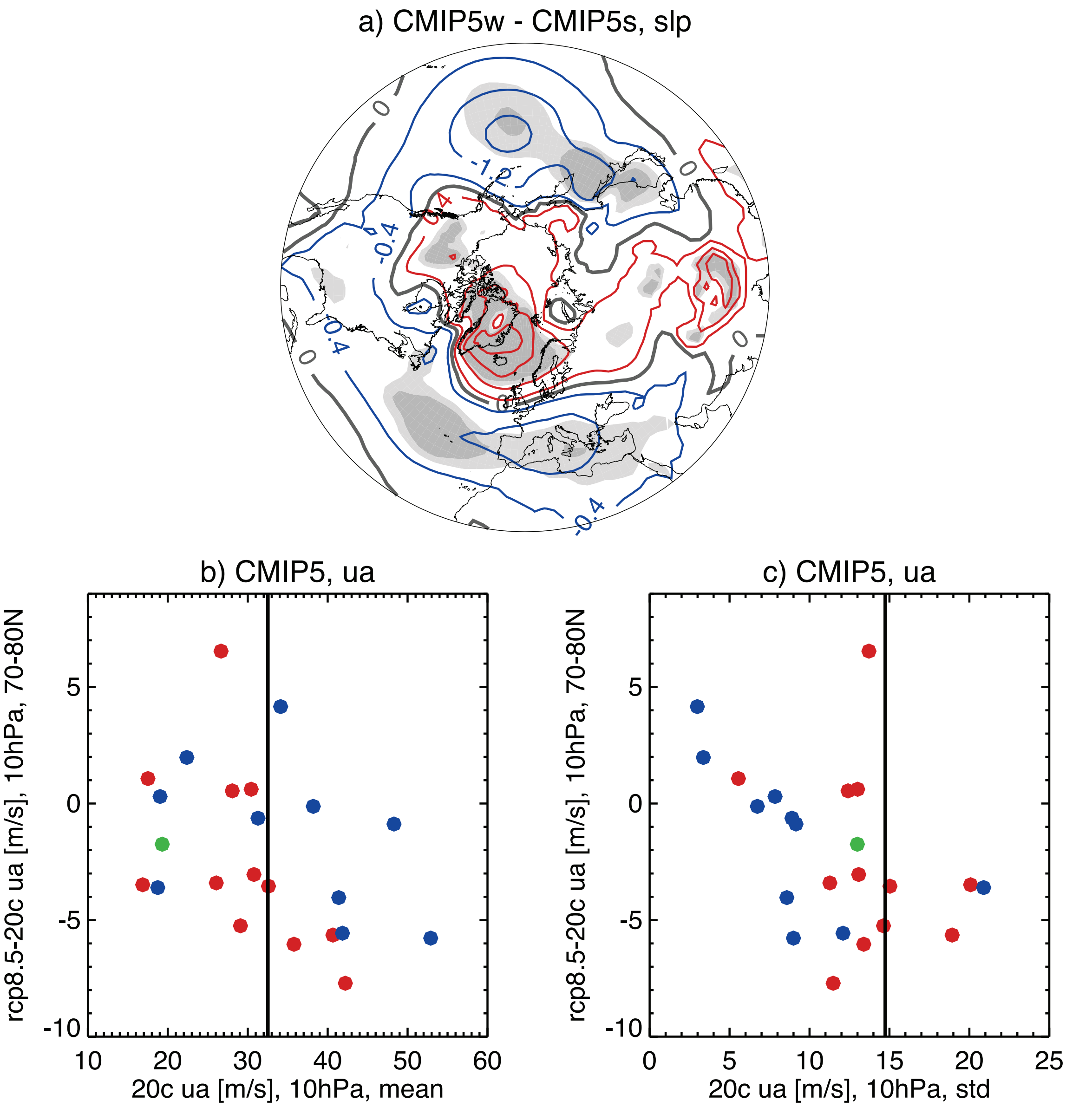
a) CMIP5w - CMIP5s, slp
0
-1.2
-0.4
0.4
b) CMIP5, ua
c) CMIP5, ua
rcp8.5-20c ua [m/s], 10hPa, 70-80N
5
0
-5
-10
10
20
30
40
50
60
20c ua [m/s], 10hPa, mean
0
5
10
15
20
25
20c ua [m/s], 10hPa, std

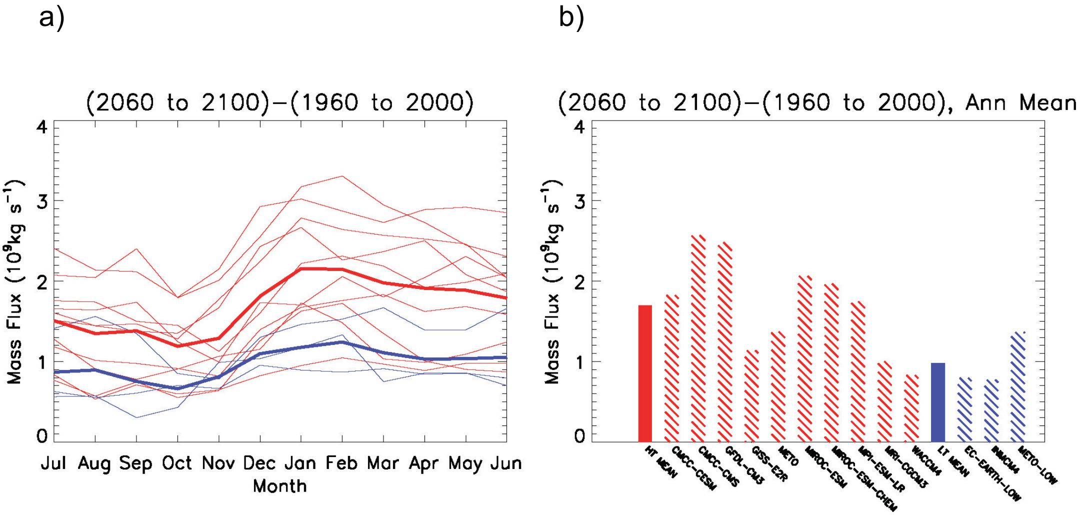
a)
(2060 to 2100)−(1960 to 2000)
Mass Flux (10^9kg s^{-1})
0
1
2
3
4
Jul
Aug
Sep
Oct
Nov
Dec
Jan
Feb
Mar
Apr
May
Jun
Month
b)
(2060 to 2100)−(1960 to 2000), Ann Mean
Mass Flux (10^9kg s^{-1})
HT MEAN
CMCC-CESM
CMCC-CMS
GFDL-CM3
GISS-E2R
METO
MIROC-ESM
MIROC-ESM-CHEM
MPI-ESM-LR
MRI-CGCM3
WACCM4
LT MEAN
EC-EARTH-LOW
INMCM4
METO-LOW

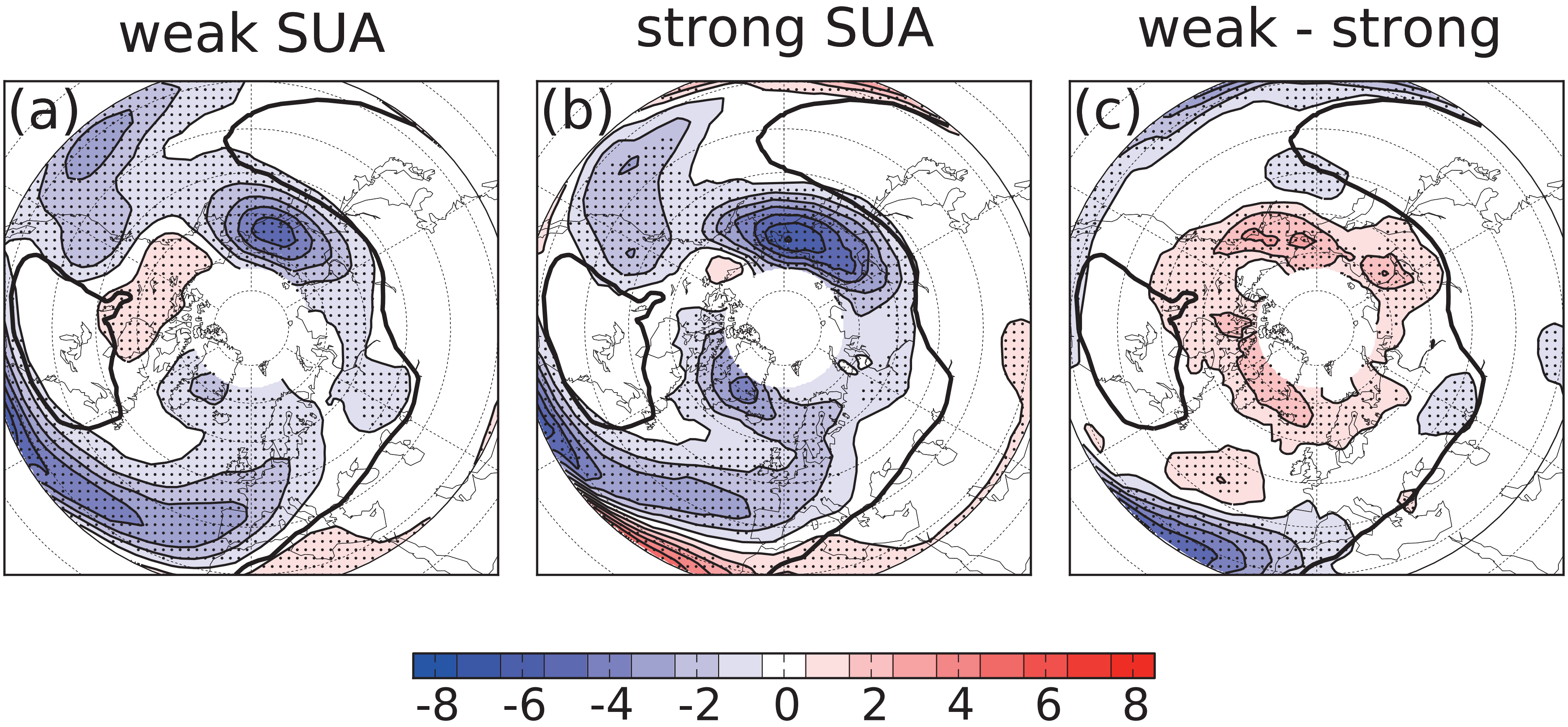
weak SUA
strong SUA
weak - strong
(a)
(b)
(c)
-8
-6
-4
-2
0
2
4
6
8

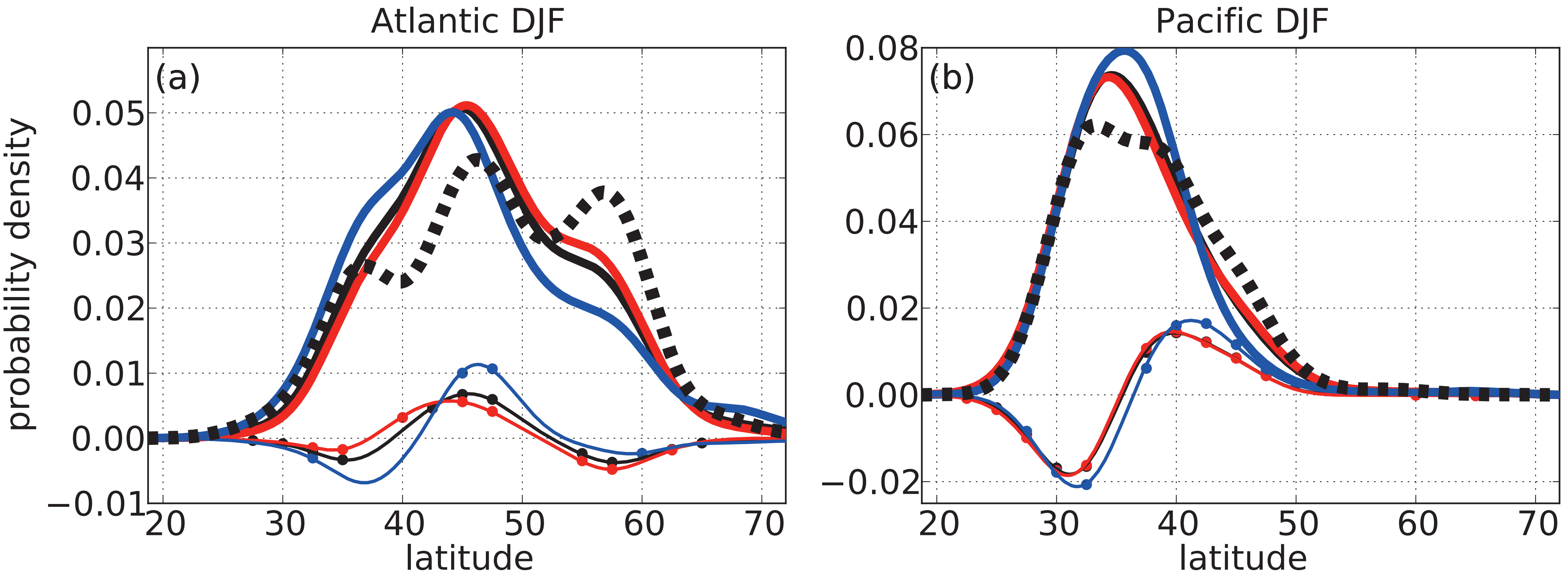

Atlantic DJF
Pacific DJF
(a)
(b)
probability density
latitude
latitude
0.05
0.04
0.03
0.02
0.01
0.00
−0.01
0.08
0.06
0.04
0.02
0.00
−0.02
20
30
40
50
60
70

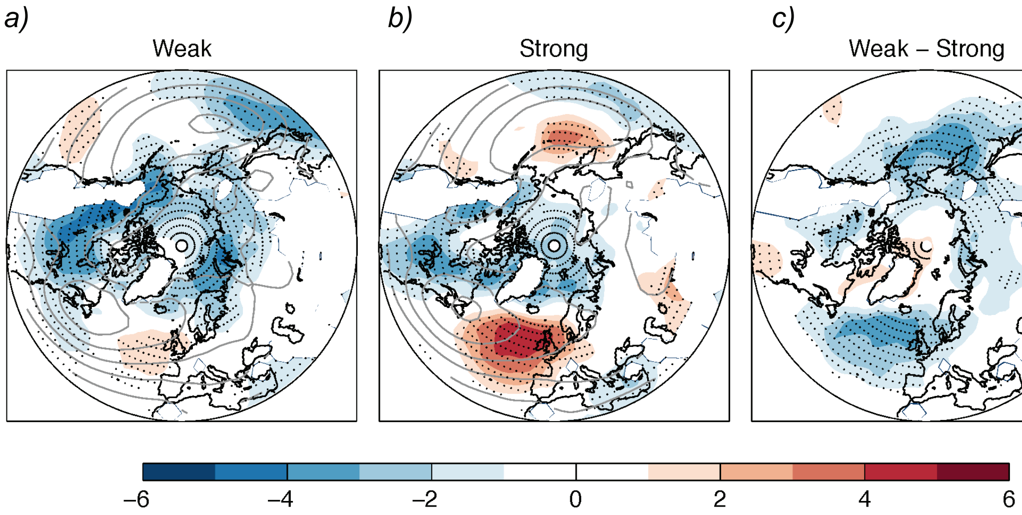

a)
Weak
b)
Strong
c)
Weak – Strong
−6
−4
−2
0
2
4
6

a)

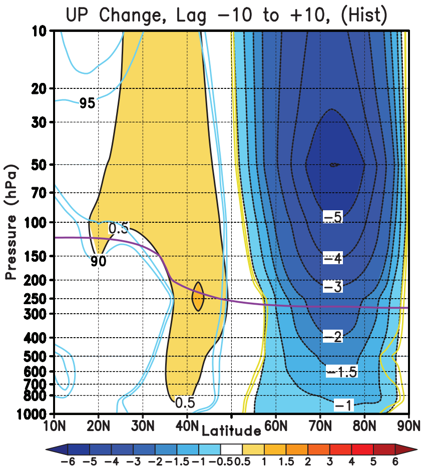
UP Change, Lag −10 to +10, (Hist)
Pressure (hPa)
Latitude
10 20 30 50 70 100 150 200 250 300 400 500 600 700 800 1000
10N 20N 30N 40N 60N 70N 80N 90N
−6 −5 −4 −3 −2 −1.5 −1 −0.5 0.5 1 1.5 2 3 4 5 6

b)

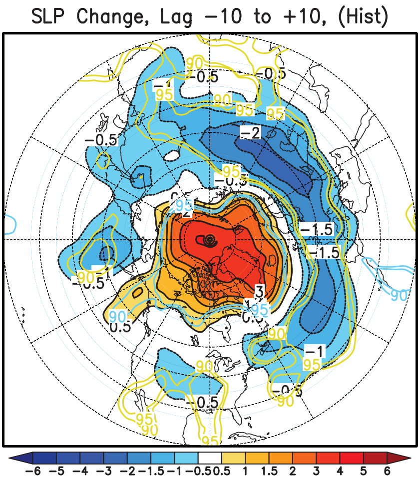
SLP Change, Lag −10 to +10, (Hist)
−6 −5 −4 −3 −2 −1.5 −1 −0.5 0.5 1 1.5 2 3 4 5 6

c)

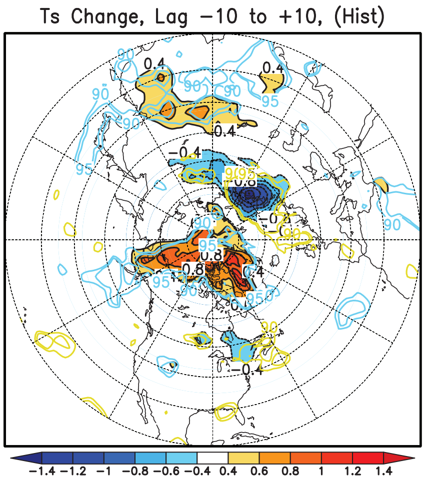
Ts Change, Lag −10 to +10, (Hist)
−1.4 −1.2 −1 −0.8 −0.6 −0.4 0.4 0.6 0.8 1 1.2 1.4